Decomposition of Fundamental Lamb wave Modes in Complex Metal Structures Using COMSOL®.

R.A. Malaeb, E.N. Mahfoud, M.S. Harb*
Laboratory of Smart Structures and Structural Integrity, Department of Mechanical Engineering, American University of Beirut, Beirut, Lebanon
* Corresponding: mh243@aub.edu.lb

Abstract

Structural Health Monitoring Systems are being highly investigated to evaluate the health of a structure and detect any damages occurring in real time. Such systems require intensive data analysis which gets even more intricate when working with complex structures due to undesirable boundary wave reflections. Guided wave signals are normally mixed with reflected signals from structural boundaries which makes it difficult to identify and localize damages. In this work, COMSOL Multiphysics® was used to better understand the reflection phenomenon of guided Lamb waves in complex isotropic structures and how such waves could be studied to characterize a damage. Aluminum plates with different sizes and shapes were modeled using the Structural Mechanics Module and coupled with different piezo-ceramic transducers acting as actuators and sensors to stimulate and sense first order Lamb wave modes. Recorded signals were analyzed and decomposed into incident, reflected, and mode changing packets. Simulation models were validated by experimental measurements and good agreement was achieved. Such analysis is a step forward to better understand the propagation of incident and reflected Lamb waves in thin solid structures.

Introduction

Waves travel through solid material while transferring disturbing energy that carries various information regarding the medium without transporting any mass in it. These propagations cause deformations that are reversed by "Restoring forces" [1, 2]. The carried information by these waves is often used in ultrasonic non-destructive testing (NDT) for material characterization and damage detection. Aerospace and automotive industries are expected to increasingly use these techniques in the upcoming years to detect damages in their complex structures [3]. One of the most reliable tests in research applications is the use of ultrasonic Lamb waves in thin-plate structures.

Lamb waves are known for their presence in thin solid plates. Mathematical physicist, Horace Lamb, first described these waves in 1917 as elastic waves [4] causing particles to move in- and out-of-plane (parallel and normal) with respect to the direction of propagation. These waves travel across the plate by reflecting off the upper and lower boundaries of thin-like structures. Two sets of infinite Lamb wave modes are thus generated making the properties of these waves very complex. In the last two decades, the increase of computational method capabilities allowed researchers to understand Lamb waves better and their usage thus increased in NDT applications. Draudviliene and Mažeika [5] and Park et al. [6] showed the importance of decomposing lamb waves modes in aluminum plates through different techniques including spectrum decomposition and group velocity and amplitude ratio rules, respectively. Harb and Yuan [7, 8] have also demonstrated experimentally, theoretically, and computationally using COMSOL the characterization of Lamb waves in isotropic plates using noncontact air-coupled/laser ultrasound method. Usage of Lamb waves for structural health monitoring (SHM) and damage detection by scattered waves' theory was also presented by various studies including Ghadami et al. [9] and Dushyanth et al. [10].

Several other authors worked on the transmission and reflection of Lamb waves from free boundaries of thin plates. Santhanam and Demirli [11] decomposed the signals of edge reflected obliquely incident Lamb waves in semi-infinite plates using collocation method. Muller et al. [12] used post-processing methods on the S_0 mode to study the reflections in aluminum plates using pitch-catch configuration from multiple Lead-Zirconate-Titinate transducers (PZTs) that are placed radially to form a circular network. Gerardin et al. [13] also showed the increase of the negative reflection from a free edge using Lamb waves in thin aluminum plates.

This work studies the behavior of the first order symmetric (S_0) and anti-symmetric (A_0) Lamb wave modes in flat, single-side bent, and two-side bent thin aluminum plates experimentally and Numerically using COMSOL Multiphysics [14]. The results from COMSOL Structural Mechanics Module are compared against each other to determine the effect of each bent boundary on the propagating waves. They are also compared with their respective experimental

counterpart to evaluate the accuracy of COMSOL in predicting reflected waves from boundaries or damages. The current study, modelled in 3-D, shows contours of the wavefields representing the wave velocity components for each plate to trace and demonstrate each wave packet.

The paper starts by briefly describing the basics of Lamb waves and their behavior in thin isotropic plates. Then the experimental setup and materials used are presented followed by an explanation of the numerical model using COMSOL. The behavior of the waves in simple and complex metallic structures is analyzed by presenting and comparing the acquired signals from different case studies in COMSOL and experimental validation. A damaged plate case is also presented and results analyzed to predict the accuracy of a COMSOL *Digital-Twin* structure to a real structure. Future work including the study of a complex carbon fiber composite wing spar will be conducted.

Fundamentals of Lamb Waves

SHM systems using piezoelectric transducers are usually based on two main wave paths studied which are the directly arrived signal and reflections from edges, bent edges and damages. It is difficult to separate these wave paths experimentally especially since the boundary reflections makes it hard to localize or identify the damage. Lamb waves are dispersive waves which means that the wave velocity varies with the frequency and the plate's thickness, generating different wave modes anti-symmetric A_i where i=0,1,2,3, etc. and symmetric wave modes S_j where j=0,1,2,3, etc. The symmetric wave modes have in plane direction parallel to the wave propagation direction while the anti-symmetric modes have a particle motion perpendicular to the direction of the wave propagation. Reflections of the modes become difficult especially with high frequencies since each mode is split into more than one mode after reflection from the boundaries. However, for low frequencies where the only existing modes are A_0 and S_0 the reflection of A_0 remains A_0 with the same angle of incident and S_0 is split into S_0 and shear wave (SH_0) modes with the S_0 having the same reflected angle as the incident and that of SH0 is smaller than the angle of incidence of S_0. Harb and Yuan [7] discussed that Lamb waves can be effectively modeled by using traction-free surface boundary conditions on the equation of motion and that introduces the dispersion phenomenon. This phenomenon for a plate placed in vacuum bounded by surface layers $z = \pm\frac{h}{2}$ where h is the plate thickness and extended infinitely in both the x and y directions for a linear, homogenous and isotropic elastic plate is

$$\frac{\omega^4}{C_T^4} = 4k^2q^2\left[1 - \frac{p\tan\left(\frac{ph}{2}+\gamma\right)}{q\tan\left(\frac{qh}{2}+\gamma\right)}\right]$$

where γ represent the S and A lamb wave modes for values 0 and $\frac{\pi}{2}$ respectively.

$$p^2 = \frac{\omega^2}{C_L^2} - k^2 \quad \text{and}$$

$$q^2 = \frac{\omega^2}{C_T^2} - k^2$$

where k is the wave number, ω is the angular frequency, C_L and C_T are respectively the longitudinal and transverse velocities of the bulk material.

Experimental Setup

The experiment was conducted on three aluminum 1050 plates of different sizes and geometries, as shown in Figure 1 with the following properties: E = 71 GPa, υ = 0.33, and ρ = 2710 kg/m^3. A set of five circular PZTs, each having a dimension of 10 mm diameter and 1 mm thickness, were bonded to the surface of each plate along the horizontal line of symmetry as shown in the same figure in a *pitch-catch* configuration.

A Keysight 33500B signal generator was used to generate a low bandwidth five-peak Hann-windowed tone-burst signal which was fed into a broadband linear amplifier (Piezo System Inc. EPA-104) to overcome Lamb wave attenuation. The amplified signal plotted in Figure 2 was then applied to the PZT discs. Upon excitation, Lamb waves were generated in the plate which were then measured by the other PZT sensors and recorded using a Keysight InfiniiVision DSO-X 3024A digital storage oscilloscope. The full experimental setup is shown in Figure 3.

Based on the theoretical group velocity dispersion curve and amplitude tuning curve found experimentally and using Wavescope Software [15] shown in Figure 4, the magnitudes of the firstly arrived A_0 and S_0 waves were compared to each other with respect to the center frequency of the excited waves. It was found that at around 90 kHz the A_0 reached high amplitude when compared to S_0 while at 200 kHz the S_0 mode reached a maximum where A_0 was diminished. Based on this result and for the ease of the experiments, the chosen frequencies for our study were 100 kHz and 200 kHz.

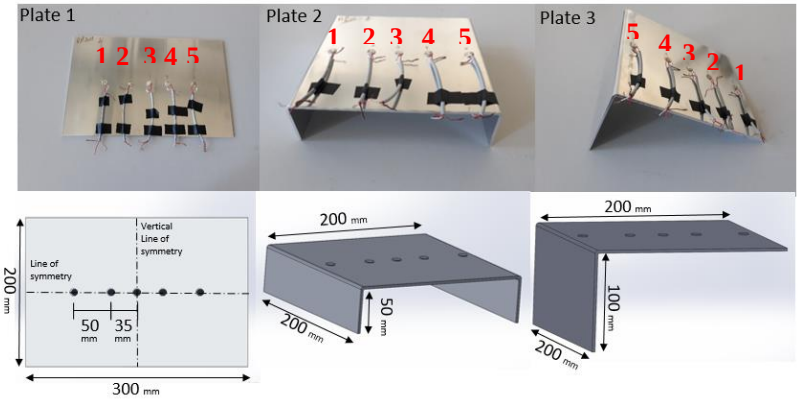

Figure 1. Actual and modelled Aluminum 1050 plates

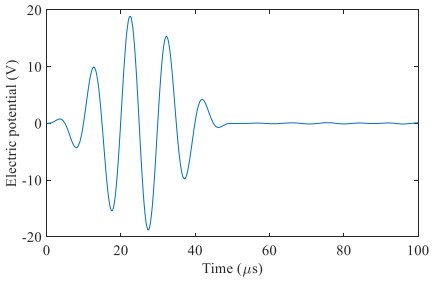

Figure 2. Input five-peaked Hann-windowed tone-burst signal

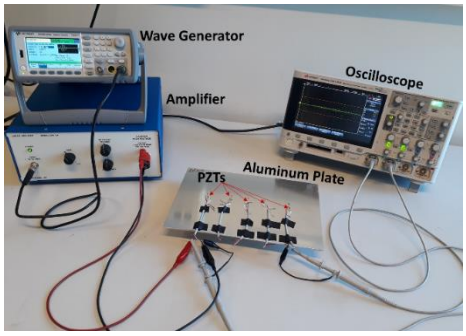

Figure 3. Experimental setup

In each of the three plates, PZT 2 from the left side of the plate acted as an actuator while PZT 5 measured the propagating wave. The computed signals at each frequency (100 and 200 kHz) were then recorded and plotted against each other. Data from Waveform Revealer [16] were treated as baseline signals since it does not account for any reflections nor attenuation from the material and present PZTs. Plate 1 was studied to understand the reflections from free-edge boundaries while data from Plates 2 and 3 were used to characterize reflected waves on bent edges in metallic plate-like structures.

Figure 5 shows the difference between the actual signal (experimental), the numerical model (COMSOL) and the theoretical signal (Waveform Revealer). The latter is based on the diameter of the two PZTs, the actual distance between them, the plate

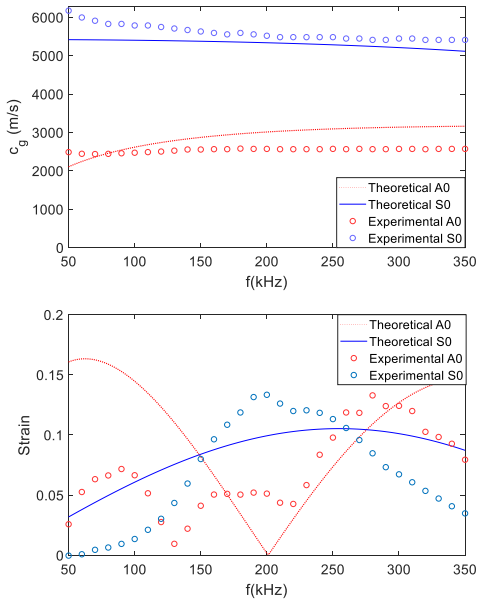

Figure 4. Group velocity dispersion curve (top) and amplitude tuning curve (bottom) of Aluminum 1050 plate

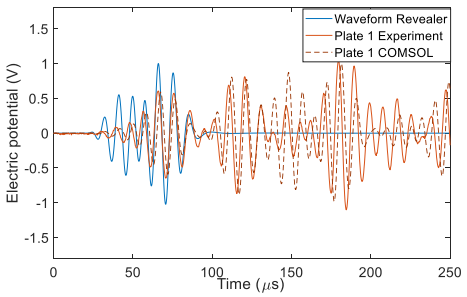

Figure 5. Experimental and COMSOL results compared to Waveform Revealer results for plate 1 at 100kHz

thickness and the material properties. It is noticed that the signals from the numerical model and experiments were very close when normalized with respect to the maximum Voltage. The theoretical signal however, had a higher amplitude especially for the first received mode (S_0) which was mainly due to the presence of two PZT discs between the actuator and sensor in the experiment and COMSOL model which affects the amplitude of the propagating signal.

Numerical Model

In order to analyze and visualize the interaction of Lamb waves with boundaries, a guided wave propagation was emulated based on a three-dimensional (3D) finite element software, COMSOL Multiphysics was used for this analysis. The plates and PZTs used in the experiments were 3D modeled using Structural Mechanics Module with Piezoelectric Solid Interaction physics. The material of the plate and PZT discs were chosen as Al-1050 and PZT-5H, respectively.

The actuating PZT discs attached to the plates were actuated by the same input signal generated by the wave generator in the experiment section. The amplitude was modified to match the experimental input amplitude so that the results can be easily compared. The signal was applied to the PZT face as an electrical potential.

Mesh

The geometry of each plate was divided into three different regions as shown in Figure 6. Most of the plate was considered to have quadrilateral elements that was mapped and swept to have an optimum computational time; since these cubic elements have the best quality at lower number of elements. The PZTs had to be taken as free tetrahedral elements since they are considered as complex geometries. Hence, the region between the two had to have nodes that match both previous regions, which is why it was specified as triangular elements to bond with the tetrahedral elements above it and swept into prism elements within the thickness to bond with the hexahedral elements next to it.

One of the most significant parameters in the implementation of COMSOL is the mesh density. Increasing the density improves the accuracy, but increases the computational complexity of the model. Different maximum element sizes were tested in order to choose the optimal mesh density as presented in Table 1. In the case of wave characterization, the maximum element size (Δx_{max}) should be chosen in accordance with the wavelength of the excited wave (λ) according to the equation $\Delta x_{max} = \lambda/r$ where r = 1, 2, 3, n is the wavelength-element size ratio. The wavelength was calculated based on the following equation $\lambda = v/f$ where v is the excited wave phase velocity in (m/s) and f is the frequency of excitation in (kHz). For an excitation wave of 100 kHz center frequency, the wavelength was

$$\lambda_{100} = \frac{v}{f} = \frac{1551 m/s}{100\ kHz} = 15.51\ mm.$$

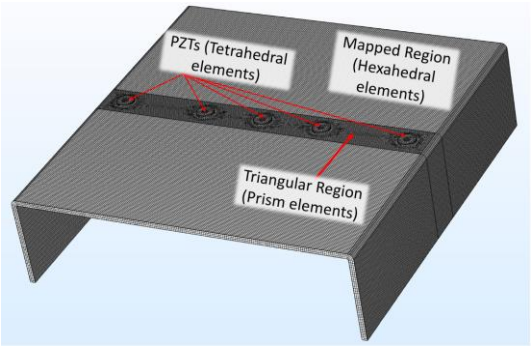

Figure 6. Mesh plot and meshed regions of Plate 2 in COMSOL model

According to the obtained results, it has been realized that the data was varying as the wavelength-element size ratio varied between 10 and 20. It is known that the element size and the computational time are inversely proportional and based on the results, the chosen mesh was of ratio 15 which resulted in an acceptable steady solution. In addition, the time step used in the COMSOL model was $2.5 \times 10^{-7}\ sec$ which is far below the reported value used in literature [17].

Results

Although the experiment was based on two PZTs, an actuator and a sensor, the experimental plates contained five PZTs each. Hence, the COMSOL model was built with the additional PZTs to efficiently represent the experimental plates. The absence of the un-used PZTs affected the results obtained as shown in Figure 7. Therefore, for the rest of the numerical simulations, all the PZTs were considered to mimic their effect in the experiments.

Table 1. Maximum element size and number of elements

	r	Δx_{max} (mm)	Elements
Mesh 1	10	1.551	99165
Mesh 2	12	1.292	134080
Mesh 3	14	1.107	178105
Mesh 4	15	1.034	202816
Mesh 5	16	0.968	228197
Mesh 6	17	0.912	256669
Mesh 7	20	0.775	353236

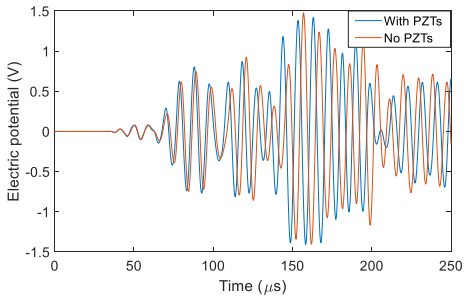

Figure 7. The effect of additional PZT discs placed between actuator and sensor

Two sets of results were obtained for each of the three plates from the two used frequencies. For each plate and at each excitation frequency, the experimental and numerical results were plotted as shown in Figures 8, 9 and 10. In all plates at 100 kHz, the two signals matched to a great extent except for the third packet which as shown in the figures had a higher amplitude in COMSOL. As for the 200 kHz excitation frequency, the results show a good match between the direct incident signals but a variation of amplitudes for the reflected wave packets.

The difference in the third packet at 100 kHz from experimental to numerical data is mainly due to the fact that this reflection passes through all five PZTs while returning from the left to the right side. In reality, damping from PZTs causes more attenuation in the signal and therefore reduces the amplitude of this packet. The same thing could be said for the fourth packet of plate 3 at this frequency. As for the 200 kHz frequency, since S_0 was the more dominant mode, and since it has a much higher speed than A_0, the signal's wavelength is lower and therefore the effect of the PZTs is even higher in real life situations. COMSOL might need additional information about the damping of the air around the plate and the glue attached to the PZTs which also causes changes to the sensed signals.

The wavefields of the velocity obtained using COMSOL, in *x*, *y* and *z* directions representing in- and out-of-plane velocities for the waves, simplified the decomposition of the signal and the packets of the collected signal and their sources can be identified easily. The sensed signal from PZT 5 excited by PZT 2 at 100 kHz is plotted in Figure 11. It is noticed that the first packet is a combination of both S_0 and A_0 modes of the first arrived signal. Their out-of-plane wavefield (velocity contours in the *z*-direction) is shown in Figure 12 where S_0 and A_0 are clearly noticed and marked. The second packet is the reflected signal of the A_0 mode from the top, bottom and right side in addition to a reflected S_0 signal from the left side of the plate. The third packet shows the first reflection of A_0 from the left side of the plate and the fourth packet refers to the second reflection of A_0 from the top and bottom sides. Other reflections from different angles could also be present but with much smaller amplitudes and could not be clearly seen from any of the plotted wavefields. It is thus noticed that the complexity of measured Lamb waves is due not only to multi-mode excitation but to free-edge reflections in small plate.

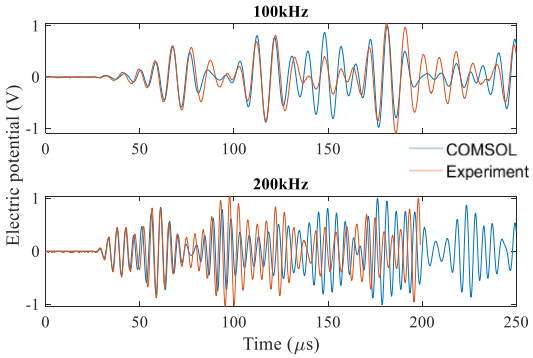

Figure 8. Experimental vs COMSOL results for both frequencies of 100 and 200 kHz for plate 1

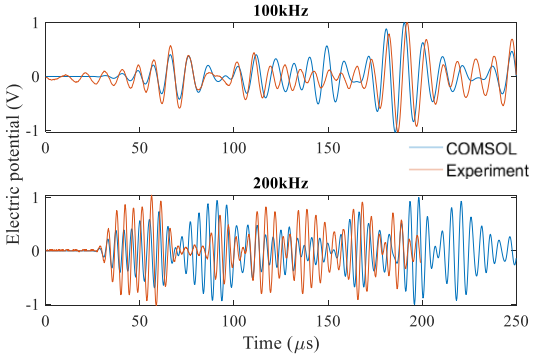

Figure 9. Experimental vs COMSOL results for both frequencies of 100 and 200 kHz for plate 2

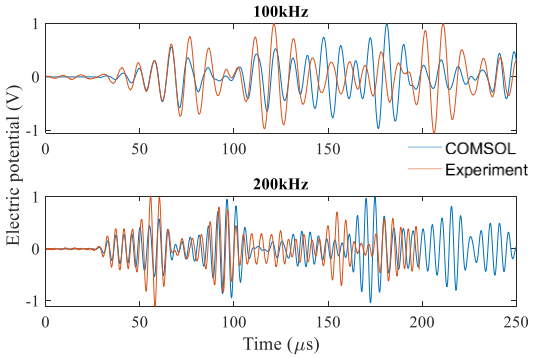

Figure 10. Experimental vs COMSOL results for both frequencies of 100 and 200 kHz for plate 3

To study the effect of the bent edge(s) in plates 2 and 3, the signals obtained from COMSOL at 100 kHz excitation frequency were compared to plate 1 to detect their influence on the signal and separate it from the boundary reflections. The wave envelopes in each plate were drawn as shown in Figure 13 and 14. The envelopes matched greatly except for two main time intervals. These intervals are investigated through the wavefields of each plate in the *z*-direction, since A_0 is dominant in this frequency. The second packet or P2 in Figure 14 shows higher amplitude for plate 1 when compared to the two other plates. The reason behind this difference in amplitude is shown in Figure 15 where the reflection of A_0 from the right bent edge shown from the wavefield of plate 2. This reflected signal diminishes the effect of the transmitted one all the way to the right edge which is full in capacity in plate 1 and makes the amplitude of the right reflection from A_0 at P2 time interval higher in plate 1.

The second difference is shown in the fourth packet or P4. This time plates 1 and 3 have the same low amplitude compared to plate 2. The first part of this packet is from the second reflections of A_0 from top and bottom sides, this is the same for all plates. However, the second part of this packet is only noticed in plate 2 due to the two bent edges and the reflected and transmitted waves from both edges. Figure 16 shows the four reflections that hit the sensor at this time interval which are only detected in plate 2 at this specific time. Plate 1 does not have the bent edges at all and plate 3 has a longer distance at its right side bent edge which also does not allow these reflections to hit the sensor at the time given. This analysis from COMSOL allowed the bent edges and their effect on transmission and reflections to be shown and studied more profoundly than only theoretically.

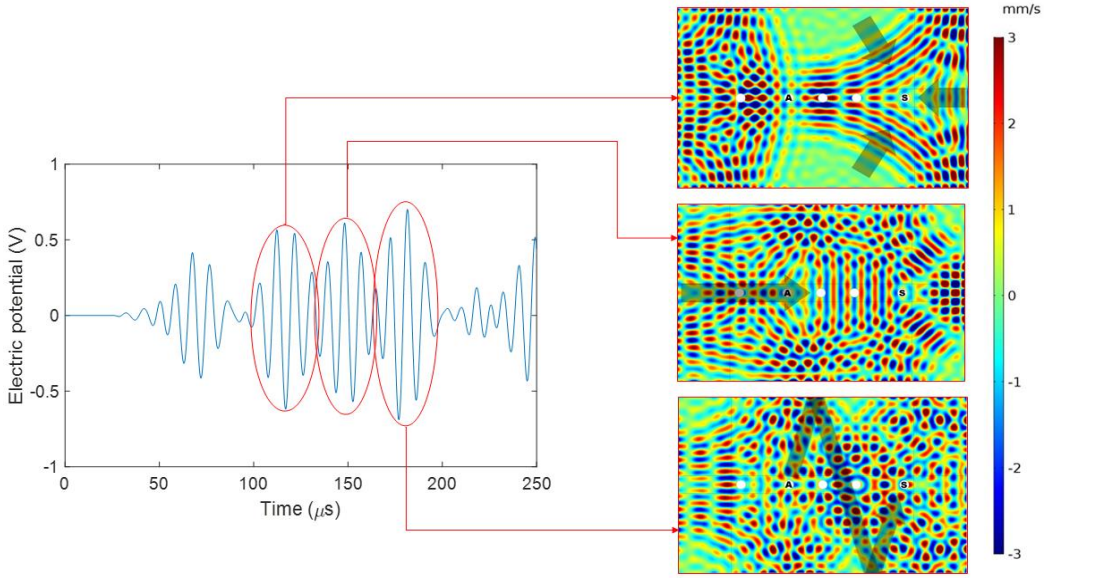

Figure 11. Sensed signal in Plate 1 divided into packets where every packet is specified based on the obtained wavefield

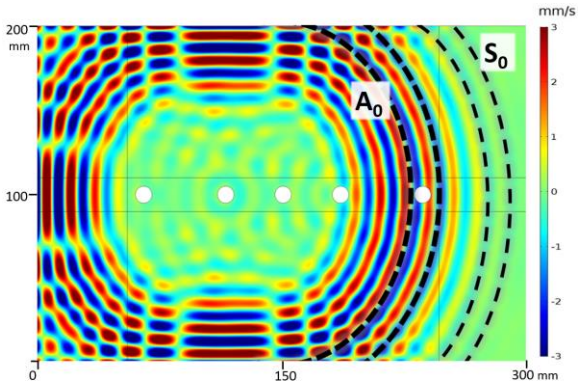

Figure 12. Out-of-plane velocity wavefield showing excited S_0 and A_0 modes

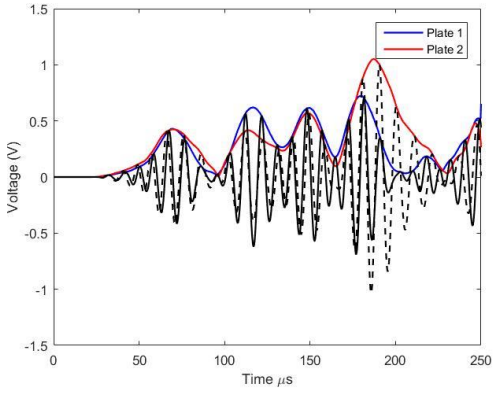

Figure 13. Measured signal and envelope tracing

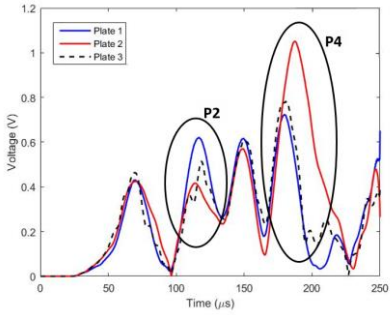

Figure 14. Measured signal envelopes for each plate

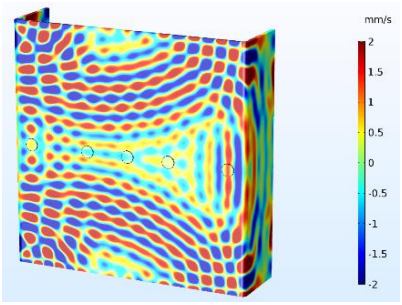

Figure 15. Reflection and transmission wavefield from the right side bent-edge in Plate 2

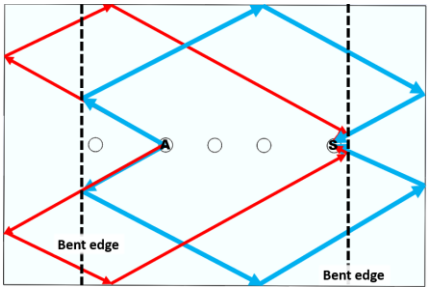

Figure 16. Four pathway reflections in plate 2

Damage Detection

A damage in plate 1 was represented numerically by a 20 mm x 20 mm x 2 mm groove located in the middle of the plate below the third PZT as shown in Figure 17. Similar analysis to the previous study was also used on the damaged plate with an excitation signal of 100 kHz center frequency. The measured signal by the sensing PZT 5 were plotted in Figure 18 against the signal from the pristine plate and a clear change in the signal was noticed which informs of the existence of a discontinuity in the plate. The signal of the damaged plate is clearly lagging with respect to that of the undamaged plate. In addition, the second packet had a clear lower amplitude which was directly caused by the presence of this damage. Figure 19 shows how the reflection from the bottom side is not received with the reflections from the top and right sides as in previous results from plate 1. It is also important to note that wavelength of A_0 wave at 100 kHz was 15.51mm which is smaller than the embedded damage.

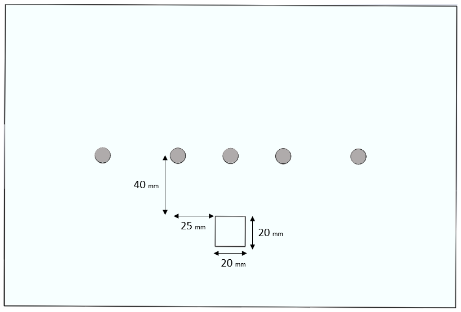

Figure 17. Plate 1 with a 20 mm x 20 mm x 2 mm grooved damage

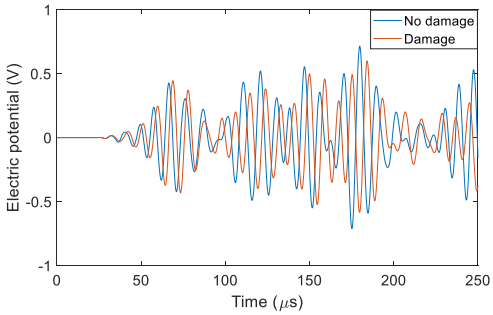

Figure 18. Results of plate 1 for a damaged plate vs an undamaged plate

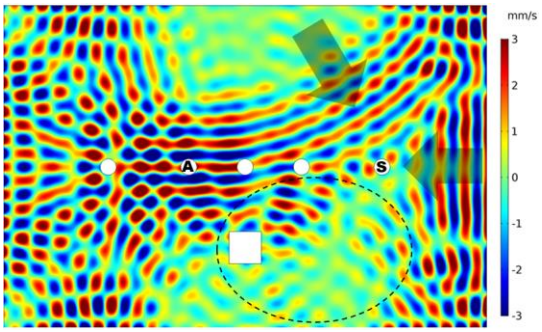

Figure 19. The received reflections at 100 μs from plate 1 with damage

Conclusion

In this paper, a COMSOL *Digital-Twin* structure is studied by comparing experimental data to numerical simulations performed on the Structural Mechanics module in COMSOL Multiphysics. Lamb waves in isotropic Aluminum plates were studied to decompose incident, reflected and scattered wave packets from the received signals. The comparison of the experimental results with that obtained from COMSOL matched to a very good extent. Every wave mode and reflected

packet was decomposed by analysing the wavefield in the out-of-plane velocity. Moreover, plates with bent edges were studied and their wavefields showed that these bends partially reflect some of the incident wave. Characterization of damage is also modelled and briefly studied to determine its effects on the received signal. Such analysis is a step forward to better understand the propagation of incident and reflected Lamb waves in thin solid structures. Further studies will be held for more complex bent structures such as a carbon fibre wing spar that includes several bent edges and discontinuities.

Acknowledgment

Recognition and gratitude are addressed to the University Research Board at the American University of Beirut for their Award # 103371. The Lebanese National Council for Scientific Research (CNRS) is also acknowledged.

References

1. Chakravorty P., "What Is a Signal? [Lecture Notes]", *IEEE Signal Processing Magazine*, **35(5)**, 175-177 (2018)
2. Rose, J. L., Ultrasonic guided waves in solid media, *New York NY: Cambridge University Press*, (2014)
3. "Ultrasonic Testing Market by Type (Time-of- Flight Diffraction, Phased Array, Immersion Testing, Guided-Wave), Equipment (Flaw Detectors, Tube Inspection, Transducers & Probes, Bond testers), Service, Vertical, and Geography - Global Forecast to 2022," *Market Research Firm*. [Online]. Available at: https://www.marketsandmarkets.com/Market-Reports/ultrasonic-testing-market-131229239.html. (2016)
4. Lamb, H., On waves in an elastic plate. Proc. R. Soc., **93**, 114–128 (1917)
5. Draudvilienė, L., & Mažeika, L., Investigation of the spectrum decomposition technique for estimation of the group velocity Lamb waves, *Ultrasound*, **66(3)** (2011)
6. Park, I., Jun, Y., & Lee, U., Lamb wave mode decomposition for structural health monitoring, *Wave Motion*, **51(2)**, 335-347 (2014)
7. Harb, M.S., Yuan, F.G., A rapid, fully non-contact, hybrid system for generating Lamb wave dispersion curves, *Ultrasonics*, **61**, 62– 70 (2015)
8. Harb, M. S., & Yuan, F., Air-Coupled Nondestructive Evaluation Dissected. *Journal of Nondestructive Evaluation*, **37(3)** (2018)
9. Ghadami, A., Behzad, M., & Mirdamadi, H. R., Damage identification in multi-step waveguides using Lamb waves and scattering coefficients, *Archive of Applied Mechanics*, **88(6)**, 1009-1026 (2018)
10. Dushyanth, N. D., Suma, M. N., & Latte, M. V., Mathematical modeling of Lamb wave scattering for structural health monitoring, *Journal of Civil Structural Health Monitoring*, **5(5)**, 743-749 (2015)
11. Santhanam, S., & Demirli, R., Reflection of Lamb waves obliquely incident on the free edge of a plate. *Ultrasonics*, **53(1)**, 271-282 (2013)
12. Muller, A., Robertson-Welsh, B., Gaydecki, P., Gresil, M., & Soutis, C., Structural Health Monitoring Using Lamb Wave Reflections and Total Focusing Method for Image Reconstruction. *Applied Composite Materials*, **24(2)**, 553-573 (2016)
13. Gérardin, B., Laurent, J., Prada, C., & Aubry, A., Negative reflection of Lamb waves at a free edge: Tunable focusing and mimicking phase conjugation. *The Journal of the Acoustical Society of America*, **140(1)**, 591-600 (2016)
14. "COMSOL Multiphysics Reference Manual, version 5.3", COMSOL, Inc, www.COMSOL.com
15. Laboratory for Active Materials and Smart Structures (LAMSS), University of South Carolina (2010) Wavescope 2.5. Available at: http://www.me.sc.edu/Research/lamss/html/software.html
16. Laboratory for Active Materials and Smart Structures (LAMSS), University of South Carolina (2012) Waveform Revealer 3.0. Available at: http://www.me.sc.edu/Research/lamss/html/software.html
17. Ghose, B., Balasubramaniam, K., Krishnamurthy, C. and Subhananda Rao, A., Two Dimensional FEM Simulation of Ultrasonic Wave Propagation in Isotropic Solid Media using COMSOL, *COMSOL Conference 2010 India* (2010)